Synthesis, Structure and Photocatalytic Dye Degradation Ability of Co(II)-Based Coordination Polymers

Weiyuan Zuo[1] · Yongfeng Fan[1] · Lijin Yang[1] · Liansheng Cui[1]

Abstract

Two Co(II)-based coordination polymers: $\{Co(L_1)(bimb)\cdot H_2O\cdot OH\}_n$ (**1**) and $[Co(L_2)(bidpe)]_n$ (**2**) ($H_2L_1 = 4$-mercaptobenzoic acid, $H_2L_2 = 4,4'$-bis(thiomethylene) dibenzoic acid, bimb = 1,4-bis(imidazol-1-ylmethyl)benzene), bidpe = $4,4'$-bis(imidazolyl)diphenyl ether), were synthesized under the condition of solvothermal and characterized by X-ray single-crystal diffraction, elemental analysis, IR spectra and thermogravimetric analysis (TGA). X-ray single-crystal diffraction analysis exhibits that **1** and **2** belong to the monoclinic crystal system, space group $P2_1$ and Cc. Complex 1 adopts a tetrahedron $\{CoN_2O_2\}$ coordination geometry and complex 2 possesses a distorted trigonal bipyramid $\{CoN_2O_3\}$ coordination geometry. Topology analysis results show that complex **1** and **2** possess a uninodal 4-connected 2D (two-dimensional) *sql* topology framework with the Schläfli symbol $(4^4\cdot6^2)$. Furthermore, the photocatalytic degradation property and mechanism of **1** and **2** for methylene blue (MB) were investigated. The results show that the band gap (E_g) of **1–2** is 2.69 eV and 2.60 eV, and the equipotential point (pH_{pzc}) of **1–2** is 4.47 and 4.40. Complex **1–2** show excellent photocatalytic degradation for MB. ·OH is the main active substance causing MB degradation.

Keywords Co(II)-based coordination polymers · Crystal structure · Photocatalytic degradation

1 Introduction

Organic dyes are widely used in textile, printing, paper, cosmetics industry, etc. They make people's life colorful and bring huge economic benefits, nevertheless, have caused enormous pollution to water resources. Methylene blue (MB) is commonly used as a representative of widespread organic dyes that contaminate textile effluents and that are lowering light penetration, photosynthesis and damage the aesthetic nature of the water surface. Methylene blue (MB) is a heterocyclic aromatic chemical compound, which has many uses in a range of different fields, like biology and chemistry. At doses of 2–4 mg kg^{-1}, hemolytic anemia and skin desquamation may occur in infants. At doses of 7 mg kg^{-1}, nausea, vomiting, chest pain, fever, and hemolysis have been described. Hypotension may occur at doses of 20 mg kg^{-1}, and bluish discoloration of the skin can occur at 80 mg kg^{-1} [1]. Therefore, it is imperative to develop effective dye removal technology. At present, the technologies of treating organic dye wastewater include adsorption method [2–4], membrane separation method [5], magnetic separation technology [6, 7], chemical method [8, 9], and biological method [10, 11]. In recent years, photocatalytic degradation by coordination polymers has provided a new way to treat organic dye wastewater [12–16].

Coordination polymers are composed of metal ions and inorganic/organic ligands assembled by coordination bonds. Aromatic polycarboxylic acids and nitrogen-containing ligands are mainly used in the synthesis of coordination polymers [17–19]. Aromatic polycarboxylic acid ligands contain multiple carboxyl groups exhibiting diverse coordination patterns, which can participate in coordination by means of single tooth, double tooth and bridge, so that the whole coordination polymer presents a rich, novel and scaffold frame structure. Since containing multiple nitrogen atoms

✉ Liansheng Cui
cls200407@163.com

1 Guangxi Colleges and Universities Key Laboratory of Regional Ecological, Environment Analysis and Pollution Control of West Guangxi, College of Chemistry and Environmental Engineering, Baise University, Baise 533000, Guangxi, China

of strong coordination ability, imidazoles are often used as the second ligand in the synthesis of coordination polymers. With the introduction of nitrogen-containing ligands, the structure of coordination polymers can be adjusted, controlled and modified to present more abundant structures and excellent properties. Coordination polymers have shown attractive application prospects in the fields of gas separation and storage [20, 21], catalysis [22–24], fluorescence sensing [25, 26] and conductive materials [27, 28].

Based on the above, two novel Co(II)-based coordination polymers were designed, synthesized and selected as photocatalyst to decompose methylene blue (MB) under UV light irradiation. The influence factors (such as pH and initial MB concentration), kinetics and mechanism of photocatalytic MB degradation and stability were also studied.

2 Experimental Section

2.1 Materials and Physical Measurements

H_2L_1, H_2L_2, bimb and bidpe were purchased from Jinan Henghua Sci. Tec. Co. Ltd., $Co(NO_3)\cdot 6H_2O$ and other solvents were purchased from the local reagent company. Infrared spectra were recorded with the Varian 640FT-IR by using KBr pellets. Elemental analysis of C, H, N were performed in the model 2400 PerkinElmer analyzer. Thermogravimetric (TG) analyses were measured on a Perkin-Elmer TGA-7 thermogravimetric analyzer under N_2 conditions from 50 to 800 °C with a heating rate of 40 °C min^{-1}. The X-ray powder diffractions (XRPD) of the complexes were collected on an Escalabmkii spectrometer 250 with an Al Kα (1486.8 eV) achromatic X-ray source. Topological analysis were performed and confirmed by the Topos program and the Systre software [29, 30]. UV–Vis absorption spectra were recorded on a UV-2700 spectrophotometer. UV–Vis diffuse reflectance data were collected over the spectral range 200–800 nm with UV-2600 spectrophotometer equipped with an integrated sphere and $BaSO_4$ was used as a reference sample.

2.2 Syntheses of Complex 1–2

A mixture of $Co(NO_3)_2\cdot 6H_2O$ (0.059 g, 0.2 mmol), bimb (0.018 g, 0.1 mmol)/bidpe (0.024 g, 0.1 mmol), H_2L_1 (0.015 g, 0.1 mmol)/H_2L_2 (0.030 g, 0.1 mmol), H_2O (5.0 mL), DMF (5.0 mL) were stirred for 0.5 h in air. And then the solution was transformed into the Teflon-lined stainless steel vessel (20 mL), sealed, and heated to 130 °C for 3 days. Subsequently, the vessel was cooled to the room temperature at the degree of 5 °C h^{-1}. Red column crystals were collected. Anal. Calcd for **1**, $C_{21}H_{22}CoN_4O_4S$ (%): C, 51.96; H, 4.56; N, 11.54. Found: C, 51.94; H, 4.59; N, 11.53. IR (KBr disk, cm^{-1}): 3651.8 (w),

3125.6 (m), 1617.6 (m), 1583.6 (s), 1570.5 (s), 1484.1 (m), 1400.3 (s), 1366.3 (s), 1293 (m), 1280 (m), 1180.4 (m), 1101.9 (s), 1083.6 (s), 850.55 (s), 777.25 (s), 743.22 (s), 666.82 (s), 628.02 (m), 566.2 (m), 523.2 (m), 478.8 (m). Anal. Calcd for **2**, $C_{34}H_{26}CoN_4O_5S$ (%): C, 61.72; H, 3.96; N, 8.46. Found: C, 61.68; H, 3.99; N, 8.44. IR (KBr disk, cm^{-1}): 3115.8 (m), 2923.6 (s), 1590.6 (m), 1580.1 (m), 1561.8 (m), 1520 (s), 1399.6 (s), 1308 (w), 1295 (w), 1240 (m), 1179.9 (w), 1109.2 (m), 1091 (m), 852.87 (m), 774.4 (m), 766.54 (m), 656.67 (m), 622.66 (w), 533.7 (w), 520.63 (w), 481.4 (w). IR spectra of complex **1**–**2** is shown in Fig. S1.

2.3 X-ray Crystal Structure Determination

Single-crystal X-ray diffraction for the suitable crystal of the complex was obtained on a Bruker Apex Smart CCDC diffractometer, using graphite-monochromated Mo-kα radiation ($\lambda = 0.71073$ Å) at 170 K. The structure was solved by direct methods using SHELXS-97 [31]. The non-hydrogen atoms were defined by the Fourier synthesis method. Positional and thermal parameters were refined by the full matrix least-squares method (on F^2) to convergence [32]. Crystallographic data for complex **1**–**2** is given in Table 1. Selected bond lengths and angles for **1**–**2** are listed in Table S1. CCDC numbers for complex 1–2 are 1585410 and 1842305.

2.4 Photodegradation Experiments of MB

1000 mL MB dye solution (C = 5, 10, 20, 40 mg L^{-1}) were prepared, respectively. Took out 100 mL MB solution (10 mg L^{-1}) into the beaker, and adjusted pH 3, 5, 7, 9, 11 using 0.1 M HCl and 0.1 M NaOH, respectively. Photocatalytic tests of complex **1**–**2** for MB degradation were performed. The photocatalytic reactions were performed by a typical process [33]: 20 mg complex **1** or **2** was dispersed in MB solutions (100 mL). The mixture was magnetically stirred in the dark for 30 min till an adsorption–desorption equilibrium, then the mixture was transferred and placed under the lighting of Hg lamp (125 W) with continuous stirring. Aliquots of the mixture samples (5 mL) were taken out with 20 min intervals, centrifuged immediately for separation of any solid. Then the sample was analyzed by UV–Vis measurement [34]. In order to ensure the rigor of the experiment, the samples were poured into the reaction system after each UV–Vis spectrophotometry test. Blank comparison experiments were taken in the absence of the catalyst.

3 Results and Discussion

3.1 Structures of Complex 1 and 2

X-ray single-crystal structural analysis reveals that **1** crystallizes in the monoclinic, space group $P2_1$. In Fig. 1a, Co(II)

Table 1 Summary of crystal data and structure refinement parameters for complex **1**–**2**

Empirical formula	$C_{21}H_{19}CoN_4O_2S \cdot H_2O \cdot OH$	$C_{34}H_{26}CoN_4O_5S$
Formula weight	485.4	661.58
Crystal system	Monoclinic	Monoclinic
Space group	$P2_1$	Cc
a (Å)	7.3941 (6)	8.1929 (8)
b (Å)	15.3043 (14)	22.083 (3)
c (Å)	9.7831 (7) Å	17.4621 (18)
α (°)	90	90
β (°)	101.315(7)	102.089 (7)
γ (°)	90	90
V (Å^3)	1085.56 (15)	3089.2 (6)
Z	2	4
D_{calcd} (Mg m^{-3})	1.485	1.422
μ (mm^{-1})	0.92	0.67
Reflections collected	9717	14,651
Data/parameters	3807/283	5315/406
$F(000)$	502	1364
T (K)	293	293
R_{int}	0.023	0.081
Final R indices [$I > 2\sigma(I)$]	$R_1 = 0.0351\ wR_2 = 0.0813$	$R_1 = 0.0716\ wR_2 = 0.1030$
R indices (all data)	$R_1 = 0.0377\ wR_2 = 0.0823$	$R_1 = 0.0994\ wR_2 = 0.1127$
Gof	1.11	1.12

cations with O atom, S atom from L_1 ligands and two N atoms from bimb ligands exhibits tetrahedral coordination sphere. Co(II) occupies the center and O, S, two N atoms lie in four vertices of the tetrahedron. The Co–O, Co–S and Co–N bonds length range are 1.991 (3)–2.307 (11) Å, and the bond angles around Co(II) ions range from 98.95 (9)° to 117.38 (15)°. One-dimensional (1D) waveform chain structure [Co-bimb]$_n$ and 1D threadiness structure [Co-L$_1$]$_n$ are formed by Co(II) cations connecting bimb ligands and L_1 ligands; Furthermore, [Co-bimb]$_n$ and [Co-L$_1$]$_n$ produce 2D network ([bimb-Co-L$_1$]$_n$) (Fig. 1b). Consequently, neighbouring [bimb-Co-L$_1$]$_n$ make 3D framework through O–H$\cdots$O hydrogen bond from dissociative H_2O moleculars and L_1 ligands (Fig. 1c). A topological analysis reveals that complex 1 is a uninodal 4-connected *sql* 2D topology framework with the Schläfli symbol $(4^4 \cdot 6^2)$, determined by TOPOS program (Fig. 1d).

X-ray single-crystal diffraction analysis shows that **2** belongs to the monoclinic system and the space group is *Cc*. The centre Co(II) ions are tetra-coordinated, coordinated by three O atoms from two L_2 ligands and two N atoms from two bidpe ligands, showing a distorted trigonal bipyramid {CoO$_3$N$_2$} configurations geometry (Fig. 2a). The Co–O and Co–N bond lengths are 2.011 (4)–2.175 (5) Å and 2.031 (5)–2.060 (5) Å, respectively, and the bond angles around Co(II) ions range from 59.9 (2) to 159.7 (2)°. 2D grid framework is formed through Co(II) ions connected L_2 and bidpe ligands (Fig. 2b), and the neighbouring 2D parallel frameworks generate a threefold interpenetrating architecture (Fig. 2c). From the view point of structural topology, the whole structure of complex **2** can be defined as a 4-connected uninodal *sql* topology framework with the point symbol of $(4^4 \cdot 6^2)$ (Fig. 2d).

3.2 Thermogravimetric (TG) Analyses

Thermogravimetric analysis is a powerful technique, which has proved to be useful in determining the lattice, and coordinated water content in the coordination polymers, and apart from this, it is useful to determine the thermal degradation behaviors, structural aspects, and thermal stability [35]. In order to evaluate the thermal stability of complex **1**–**2**, the samples were heated at a heating rate of 40 °C min^{-1} under nitrogen atmosphere over the temperature range 35–800 °C.

The thermostability of complex 1–2 were characterized by TG analyses (Fig. S2). The weight loss of complex **1** is 8.75% in the temperature range of 100–170 °C due to the loss of dissociative H_2O and OH. A major weight loss of 47.70% observed in the temperature regime 350–500 °C corresponding to collapse of the organic skeleton. For complex **2**, The weight loss of 59.30% is obviously observed in the temperature regime 300–500 °C corresponding to loss of bidpe molecules and L_2 ligands. By contrast, complex 1 has better thermal stability. In all, complex **1**–**2** show good thermostabilities under 300 °C.

Fig. 1 a Coordination environment of Co(II) in **1** (All the H atoms are omitted for clarity); **b** 2D network ([bimb-Co-L₁]ₙ) by Co(II) cations connecting bimb and L₁ ligands; **c** 3D framework of **1** through O–H···O hydrogen bond from dissociative H₂O and L₁; **d** The uninodal 4-connected *sql* 2D topology framework with the Schläfli symbol ($4^4 \cdot 6^2$) of 1 (Color figure online)
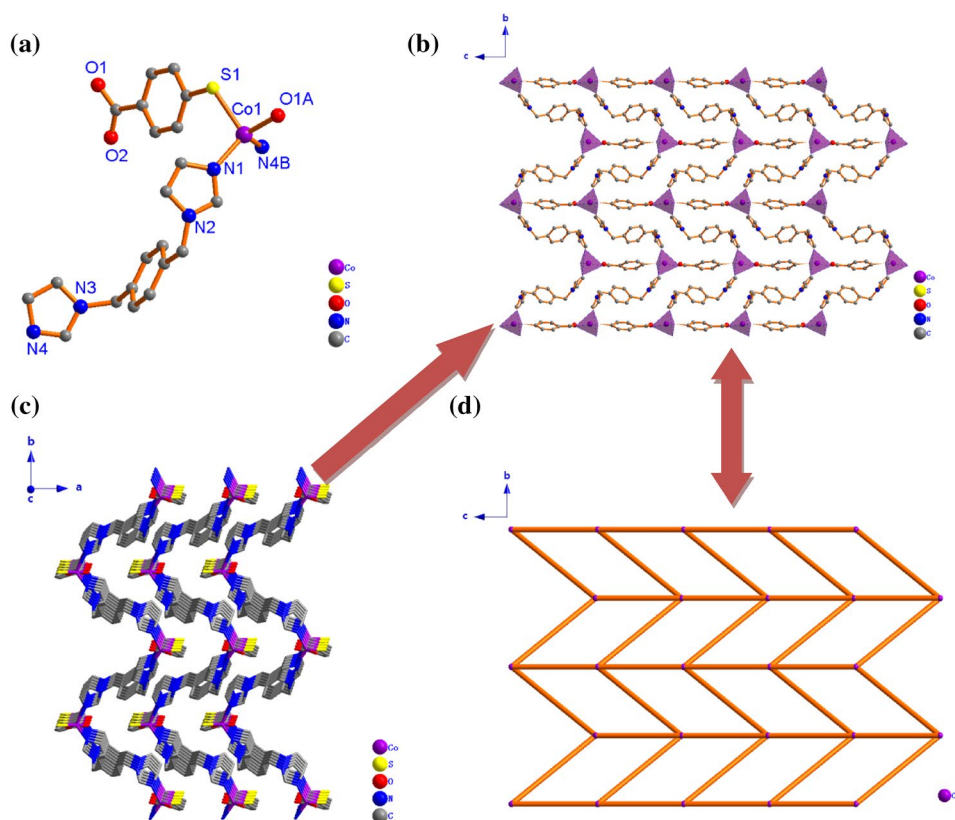
3.3 Bandgap (E$_g$)

Under the action of ligand, the energy levels of d-orbital split, then six d-electrons enter dε-orbital in the strong field, and all paired to produce diamagnetism. The electrons of dε-orbital acquired energy and can transit into dγ-orbital, and when the electrons of dγ-orbital return to dε-orbital, the energy is released, which can be measured by the instrument, namely, the d–d transition (Fig. S3).

In order to investigate the electrical conductivity of **1**, UV–Vis diffuse reflectance spectra were used to obtain their E$_g$. The E$_g$ were confirmed as the intersection point between the energy axis and the line extrapolated from the linear portion of the adsorption edge in a plot of Kubelka–Munk function *F* versus energy *E*. Kubelka–Munk function, $F = (1 - R^2)/2R$ [36], was transformed from the recorded diffuse reflectance data, where R is the diffuse reflectance based on the Kubelka–Munk theory of diffuse reflectance. The UV–Vis diffuse reflectance spectra of **1** is shown in Fig. S4. It is seen that E$_g$ of **1–2** is 2.69 eV and 2.60 eV. It indicates that **1–2** have wide band gap width and are potential semiconductor materials [37, 38], which can effectively degrade organic dyes.

3.4 Photocatalytic Degradation Capability for MB of Complex 1–2

3.4.1 Photocatalytic Degradation Analyses

The crystals of complex **1–2** were grinded before photocatalytic degradation experiment. The particle size range of complex **1–2** is from 100 to 500 μm and the morphologies are shown in Fig. 3. Under the catalysis of **1** and **2**, the UV–Vis absorption spectrum of MB degradation is shown in Fig. 4. It can be seen that the maximum characteristic absorption peak of MB is significantly reduced, which indicates that MB occurs obvious degradation. In order to show the degradation effect of MB more clearly, the C$_t$/C$_0$ versus time (t) diagram was made. C$_t$ represents the MB concentration at a certain time, and C$_0$ represents the initial concentration of MB after stirring in the dark for 30 min. As shown in Fig. 5, for complex **1**, the degradation rate of MB within 160 min is 90.88%, almost unchanged at 180 min; For complex **2**, the degradation rate of MB within 120 min is 93.44%, almost unchanged at a later time. The results show that **1** and **2** has significant photocatalytic degradation for MB. From the X-ray powder diffraction (XRPD) spectra of **1** and **2** (Fig. S5), it can be seen that the main diffraction
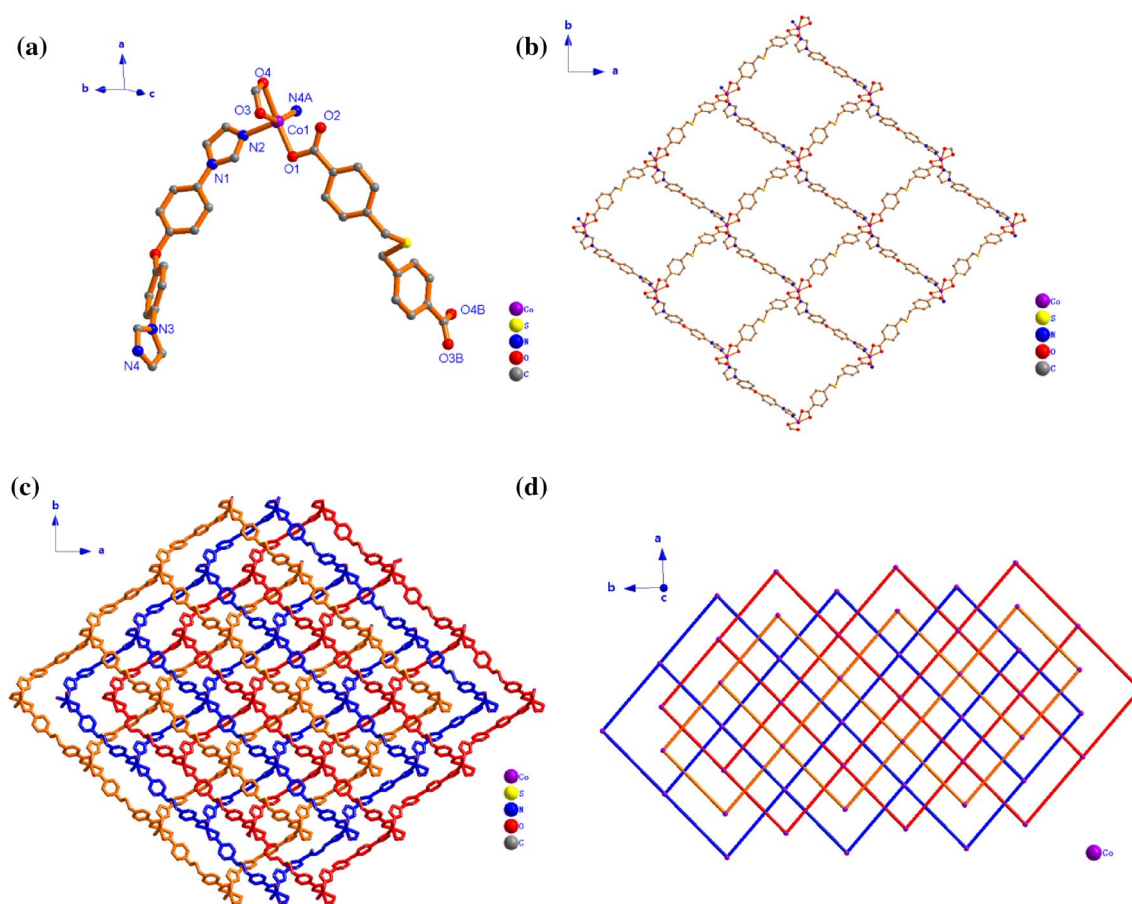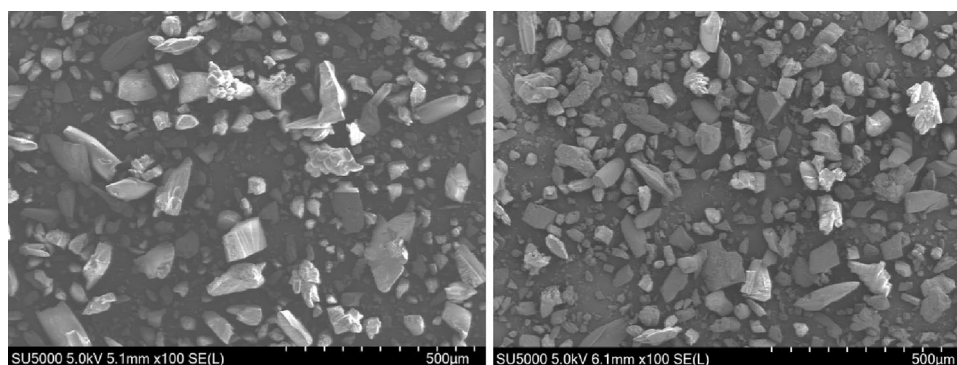
Fig. 2 **a** Coordination environment of Co(II) in **2** (All the H atoms are omitted for clarity); **b** 2D network by Co(II) cations connecting bidpe and L$_2$ ligands; **c** 3D framework of **2** through O–H···O hydro-gen bond from dissociative H$_2$O and L$_1$; **d** The uninodal 4-connected *sql* 2D topology framework with the Schläfli symbol $(4^4 \cdot 6^2)$ of complex **2** (Color figure online)

Fig. 3 SEM imagen of complex 1–2

peaks of **1** and **2** are basically unchanged before and after the reaction, which fully indicates that **1** and **2** are very stable in MB solution.

Photocatalytic degradation kinetics of **1**–**2** for MB is evaluated using first-order kinetics equation $\ln(C_t/C_0) = -kt + b$ (C_t and C_0 represent concentrations at different times (t) and initial concentration of MB, k (mg L^{-1} min^{-1}) is degradation rate constant). From Fig. 6, the degradation of MB accord with first-order kinetics model. k and R^2 values are displayed in Table S2. Obviously, the calculation result, $k_1 = 0.01709$, $k_2 = 0.02614$, $k_2 > k_1$, is in good agreement with the experimental evidence.
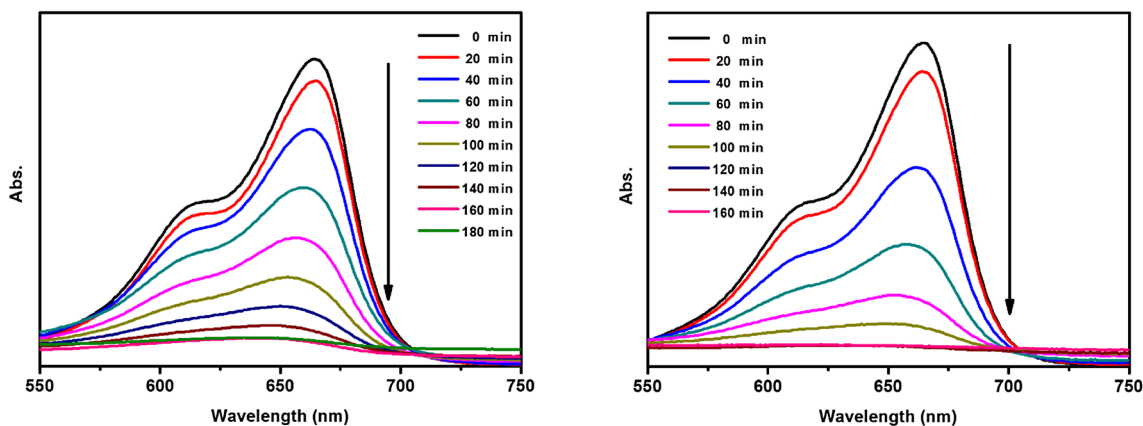
Fig. 4 The UV–Vis spectrum of MB under the catalysis of complex **1** and **2** (Color figure online)
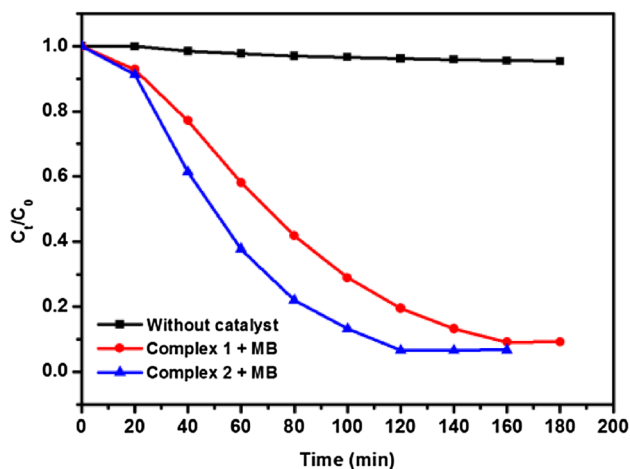

Fig. 5 Plots of concentration ratios of MB (c/c₀) against irradiation time (min) in the presence of complex **1–2** and without any catalyst under UV irradiation
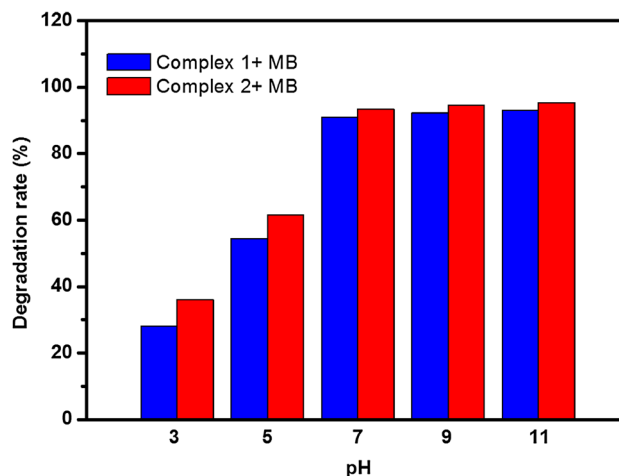

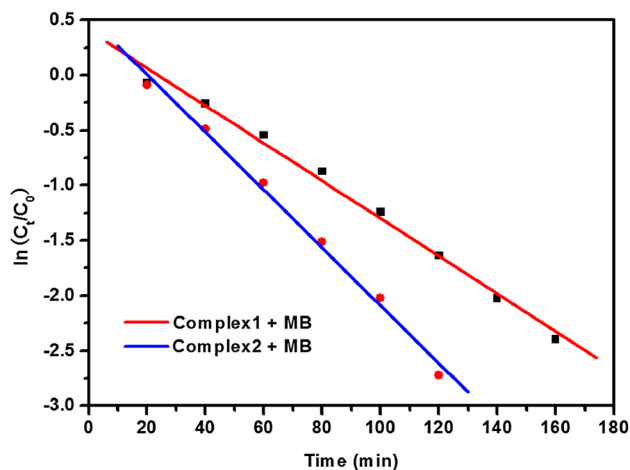**Fig. 7** Degradation rate of complex 1–2 for MB at pH 3, 5, 7, 9, 11 (Color figure online)

Fig. 6 The fitting diagram of degradation kinetics of complex **1** and **2** for MB (Color figure online)

3.4.2 Effect of pH on the Photocatalytic Activity of Complex 1–2

The pH of the MB solution was an important parameter which influenced the photocatalytic degradation reactions, since it dictates the surface charge properties of the photocatalyst and size of aggregates formed. In order to determine the effect of initial pH on the adsorption capacity and degradation efficiency of MB, the pH of MB solution was adjusted to be 3, 5, 7, 9 and 11 by using 0.1 M NaOH and HCl solutions. The MB concentration was controlled to be 10 mg L⁻¹, and the dosage of **1–2** was 20 mg. As shown in Fig. 7, The results revealed that complex 1–2 could work effectively over a pH range from 7.0 to 11.0 and showed high degradation effciency for MB. When pH 7, the degradation rate of MB has reached 90.88% and 93.44%, nevertheless, with the pH increasing, the degradation rate of MB changed little.

In order to explain the change of degradation rate of MB with pH, zero charge potential point (pH_{pzc}) is introduced. The variation curve of zeta potential of complex **1–2** with pH value is shown in Fig. 8. The intersection point of the curve and the zero electric potential is the zero charge point, and it can be known that the pH_{pzc} of **1–2** is 4.47 and 4.40. MB has the following equilibrium in solution: $MBH^{2+} \leftrightarrow MB + 2H^+$, and to its very low pKa value (less than 1), the removal of MB was due mainly to solubilization of unprotonated form of the dye [39]. The high adsorption capacity for MB may be resulted from electrostatic attraction between the negative charged adsorbent surface and the positively charged cationic dyes [40]. When pH < 7, MB mainly exists in the form of MBH^{2+}. When pH > 7, it exists mainly in MB form. When pH < 4.50, complex **1–2** have positive charge on the surface, and will generate electrostatic repulsion with MBH^{2+}, inhibiting the adsorption of **1–2** to MB, so the degradation rate of MB is greatly reduced. When pH > 4.50, complex **1–2** have a negative charge on the surface and generates electrostatic attraction with MBH^{2+}, which promotes the adsorption of **1–2** to MB, so the degradation rate of MB is greatly increased. When pH > 7, the degradation rate of MB does not change much in a limited time, because the mass of **1–2** is limited and the sites that can provide to MB are also limited.

3.4.3 Effect of MB Concentration on Degradation Rate

The influence of MB concentration on the degradation rate in complex 1–2/UV light system was evaluated. Maintained MB solution pH = 7, the addition amount of complex **1–2** was 20 mg, and the concentration of MB solution was 5 mg L^{-1}, 10 mg L^{-1}, 20 mg L^{-1} and 40 mg L^{-1}, respectively. As shown in Fig. 9, the degradation efficiencies of MB were
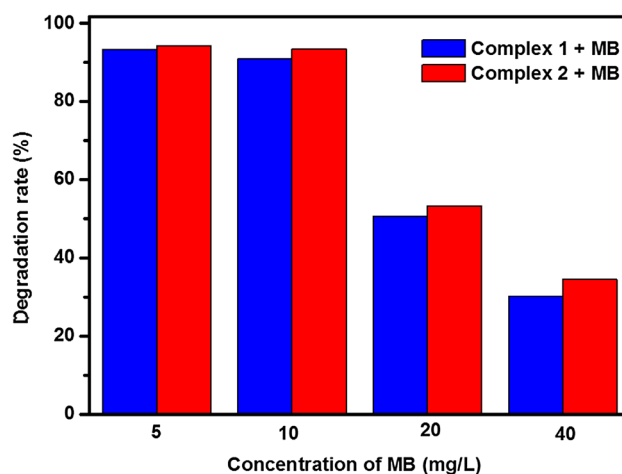

Fig. 9 The degradation rate of MB at different concentration

found to strongly depend on the MB concentration. The degradation rates of MB are not significantly different when the MB concentration is 5 and 10 mg L^{-1}. The degradation efficiencies decreased when the concentration of MB increased from 10 to 40 mg L^{-1}, which may be due to the fact that the concentration of MB increased. The increase of the dye molecules around the active sites resulted in inhibiting the penetration of light to the surface of the catalyst. Hence, the generation of relative amount of ·OH and $·O_2^-$ on the surface of the catalyst decreased with the intensity of light and irradiation times are constant.

3.4.4 Photodegradation Mechanism of MB

It's proposed that under the irradiation of the UV–Vis light, the organic ligands could be induced to generate O
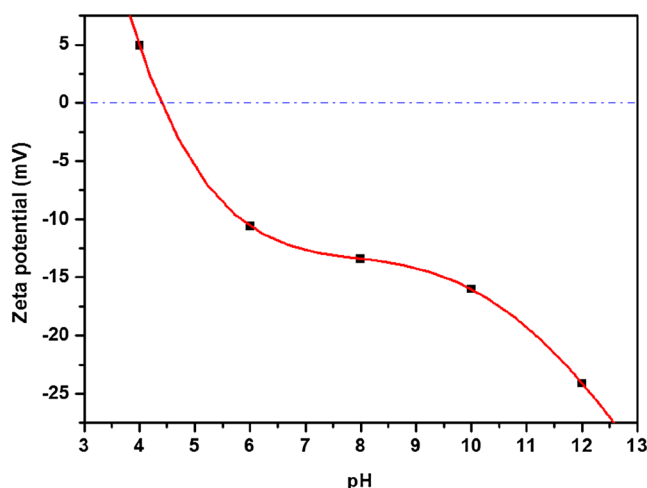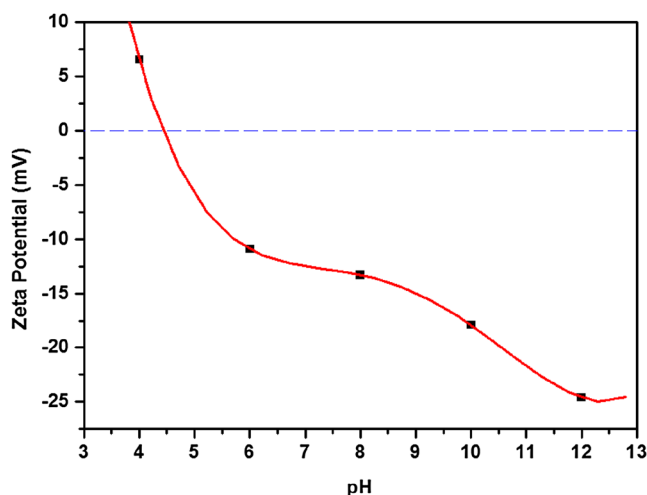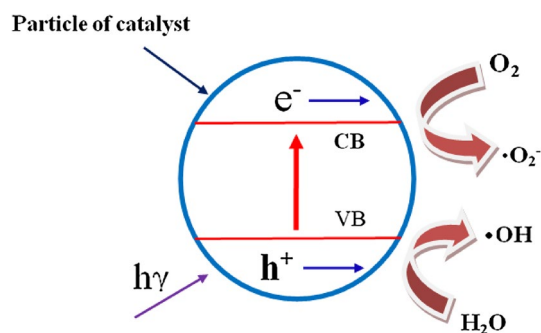

Fig. 8 Zeta potential of complex 1–2

Fig. 10 Schematic diagram of photocatalytic dye degradation of complex 1–2

or N-metal charge transfer, promoting the electron form the highest occupied orbital (HOMO) to the lowest unoccupied molecular orbital (LUMO). In order to be stable, the HOMO orbital is going to capture an electron from H_2O and O_2 molecules and to produce hydroxyl radical (·OH) and superoxide radical (·O_2^-) [41] (Fig. 10). ·OH and ·O_2^- have strong oxidation ability and can degrade dyes. So, which is the main factor to decompose certain dyes effectively and further to complete the photocatalytic process should be test. For various photocatalyst, the main specie is usually varied due to the difference in their structures. Therefore, different scavenges could be used as probes to determine the reactive species. The *tert*-butyl alcohol (TBA) was used as ·OH scavenger, an ·O_2^- scavenger, while 1,4-benzoquinone (BQ) as ·O_2^- scavenger [42]. MB solution was maintained 5 mg L^{-1}, pH 7 and the dosage of complex **1–2** was 20 mg, and the irradiation time was 160 min. As shown in Fig. S6, the degradation rate (6.45% and 2.28%) for MB of complex **1–2** by the addition of TBA in 160 min is significantly lower, with almost no change by the addition of BQ (degradation rate is 88.24% and 90.36%). The result suggests that ·OH is the main reactive specie for the degradation of MB [43, 44].

4 Conclusion

In this paper, two novel Co(II)-based coordination polymers {Co(L$_1$)(bimb)·H_2O·OH}$_n$ and [Co(L$_2$)(bidpe)] were synthesized under the condition of solvothermal. The photocatalytic degradation tests indicate that complex 1–2 can be considered as an efficient photocatalyst for degradation of methylene blue under UV light irradiation, which was confirmed by the results of detection of hydroxyl radicals (·OH). The photodegradation of MB over complex 1–2 followed first-order kinetics, and the rate constant k is 0.01709 and 0.02614 mg L^{-1} min^{-1}. Furthermore, complex 1–2 showed degradation efficiency for MB in the pH range of 7–11. Complex 1–2 were stable in aqueous solution, implying

complex 1–2 can be used repeatedly. In all, complex 1–2 can be suggested as potential photocatalyst to degrade organic pollutants.

References

1. C.C. Wang, J. Zhang, P. Wang, H. Wang, H. Yan, Desalin. Water Treat. (2014). https://doi.org/10.1080/19443994.19442013.19873881
2. N.M. Mahmoodi, R. Salehi, M. Arami, Desalination **272**, 187 (2011)
3. X.J. Li, F.Y. Qian, M. Li, Environ. Chem. **3**, 396 (2012)
4. N. Peng, K.F. Wang, C.Q. Tu, Environ. Prot. Chem. Ind. **5**, 464 (2011)
5. L.L. Fan, R.W. Lu, W.P. Chen, Environ. Sci. Technol. **S1**, 19 (2009)
6. C. Chen, P. Gunawan, R. Xu, J. Mater. Chem. **21**, 1218 (2011)
7. M. Fang, F. Mishima, Y. Akiyama, Physica C **470**, 1827 (2010)
8. M. Zhou, H. Sarkka, M. Sillanpaa, Sep. Purif. Technol. **78**, 290 (2011)
9. Y. Yao, K. Li, S. Chen, Chem. Eng. J. **187**, 29 (2012)
10. S.I. Lim, W.I. Chu, S.M. Phang, Bioresour. Technol. **101**, 7314 (2010)
11. B. Liang, Q. Yao, H. Cheng, Environ. Sci. Pollut. R. **19**, 1385 (2012)
12. L.S. Cui, J.R. Meng, Y.L. Gan, Y.C. Li, Inorg. Nano-Metal Chem. **47**, 1537 (2017)
13. L.S. Cui, X.M. Meng, Y.H. Fan, X. Li, C.F. Bi, J. Inorg. Organomet. Polym. **25**, 1490 (2015)
14. X.M. Meng, Y.C. Li, K.R. Huang, J.Q. Long, L.S. Cui, Inorg. Chim. Acta **482**, 284 (2018)
15. D.S. Liu, W.T. Chen, G.M. Ye, J.Q. Liu, Y. Sui, Inorg. Chim. Acta **477**, 84 (2018)
16. L.S. Cui, X.M. Meng, Y.G. Li, K.R. Huang, Y.C. Li, J.Q. Long, P.F. Yao, CrystEngComm **21**, 3798 (2019)
17. R. Bagade, R.G. Chaudhary, A. Potbhare, A. Mondal, M. Desimone, K. Dadure, R. Mishra, H. Juneja, ChemistrySelect **4**, 6233 (2019)
18. R.G. Chaudhary, H.D. Juneja, M.P. Gharpure, J. Therm. Anal. Calorim. **112**, 637 (2013)
19. R.G. Chaudhary, H.D. Juneja, M.P. Gharpure, J. Chin. Adv. Mater. Soc. **1**, 121 (2013)
20. Y.B. He, W. Zhou, G. Qian, Chem. Soc. Rev. **43**, 5657 (2014)
21. J.A. Mason, M. Veenstra, J.R. Long, Chem. Sci. **5**, 32 (2014)
22. W. Zhou, D.D. Huang, Y.P. Wu, J. Zhao, T. Wu, J. Zhang, D.S. Li, C.H. Sun, P.Y. Peng, X.H. Bu, Angew. Chem. Int. Ed. **58**, 4227 (2019)
23. J.W. Tian, Y.P. Wu, Y.S. Li, J.H. Wei, J.W. Yi, S. Li, J. Zhao, D.S. Li, Inorg. Chem. **58**, 5837 (2019)
24. D.D. Huang, S. Li, Y.P. Wu, J.H. Wei, J.W. Yi, H.M. Ma, Q.C. Zhang, Y.L. Liu, D.S. Li, Chem. Commun. **55**, 4570 (2019)
25. J. Ye, L. Zhao, R.F. Bogale, J. Chem. A Eur. J. **21**, 2029 (2015)
26. W.P. Lustig, S. Mukherjee, N.D. Rudd, Chem. Soc. Rev. **46**, 3242 (2017)
27. T. Yamada, M. Sadakiyo, A. Shigematsu, Bull. Chem. Soc. Jpn. **89**, 1 (2015)

28. S.S. Bao, G.K.H. Shimizu, L.M. Zheng, Coordin. Chem. Rev. **378**, 577 (2017)
29. V.A. Blatov, IUCrCompComm Newsletter **7**, 4 (2006)
30. O.D. Friedrichs, *Program SYSTRE 1.14 beta* (2007)
31. G.M. Sheldrick, SHELXTL NT, version 5.1, Program for Solution, Refinement of Crystal Structures, University of GÖttingen, GÖttingen, Germany (1997).
32. Bruker, SMART, version 5.0, SAINT-plus version 6, SHELXTL, version 6.1, SADABS version 2.03, Bruker AXS Inc.: Madison, WI (2000).
33. J. Lü, J.X. Lin, X.L. Zhao, R. Cao, Chem. Commun. **48**, 669 (2012)
34. X.L. Wang, C.H. Gong, J.W. Zhang, G.C. Liu, X.M. Kan, N. Xu, CrystEngComm **17**, 4179 (2015)
35. R.G. Chaudhary, P. Ali, N.V. Gandhare, J.A. Tanna, H.D. Juneja, Arab. J. Chem. (2016). https://doi.org/10.1016/j.arabjc.2016.03.008
36. Y. Gong, T. Wu, J. Lin, CrystEngComm **14**, 3727 (2012)
37. H.S. Liu, Y.Q. Lan, S.L. Li, Cryst. Growth Des. **10**, 5221 (2010)
38. J. Guo, J.F. Ma, B. Liu, W.Q. Kan, J. Yang, Cryst. Growth Des. **11**, 3609 (2011)
39. N. Zaghbani, A. Hahiane, M. Dhahbi, Sep. Purif. Technol. **55**, 117 (2007)
40. J.L. Gong, B. Wang, G.M. Zeng, C.P. Yang, C.G. Niu, Q.Y. Niu, W.J. Zhou, Y. Liang, J. Hazard. Mater. **164**, 1517 (2009)
41. T.T. Li, Y.M. He, H.J. Lin, J. Cai, L.Z. Dong, X.X. Wang, M.F. Luo, L.H. Zhao, X.D. Yi, W.Z. Weng, Appl. Catal. B **138**, 95 (2013)
42. Y.H. Liang, S.L. Lin, L. Liu, J.S. Hu, W.Q. Cui, Appl. Catal. B **164**, 192 (2015)
43. H.X. Yang, T.F. Liu, M.N. Cao, H.F. Li, S.Y. Gao, R. Cao, Chem. Commun. **46**, 2429 (2010)
44. X.M. Meng, C.B. Fan, C.F. Bi, Z.A. Zong, X. Zhang, Y.H. Fan, CrystEngComm **18**, 2901 (2016)